INTERNATIONAL JOURNAL FOR NUMERICAL METHODS IN FLUIDS, VOL. 13, 61–81 (1991)

TRANSIENT NATURAL CONVECTION OF LOW-PRANDTL-NUMBER FLUIDS IN A DIFFERENTIALLY HEATED CAVITY

A. A. MGHAMAD AND R. VISKANTA

School of Mechanical Engineering, Purdue University, West Lafayette, IN 47907, U.S.A.

SUMMARY

The transient convective motion in a two-dimensional square cavity driven by a temperature gradient is analysed. The cavity is filled with a low-Prandtl-number fluid and the vertical walls are maintained at constant but different temperatures, while the horizontal boundaries are adiabatic. A control volume approach with a staggered grid is employed to formulate the finite difference equations. Numerically accurate solutions are obtained for Prandtl numbers of 0·001, 0·005 and 0·01 and for Grashof numbers up to 1×10^7. It was found that the flow field exhibits periodic oscillation at the critical Grashof numbers, which are dependent on the Prandtl number. As the Prandtl number is decreased, the critical Grashof number and the frequency of oscillation decrease. Prior to the oscillatory flow, steady state solutions with an oscillatory transient period were predicted. In addition to the main circulation, four weak circulations were predicted at the corners of the cavity.

KEY WORDS Natural convection Low-Prandtl number Transient Differentially heated cavity

INTRODUCTION

When a fluid is subjected to a horizontal temperature gradient, convective motion is generated even for temperature differentials that are infinitesimally small.[1] Convection due to buoyancy is an important and often dominant mode of heat and mass transport.[2] Steady state flow and heat transfer in differentially heated cavities have been extensively investigated owing to their wide applications in fields such as solar energy utilization, nuclear reactor safety, crystal growth, metallurgy, materials processing and geophysical problems. For example, the fluid dynamic aspects of crystal growth from melts have been the topic of a number of papers, and reviews of the issues can be found in the literature.[3–5]

Transient natural convection in cavities has been studied experimentally by Pamplin and Bolt[6] and Kamotani and Sahraoui[7] using mercury and by Yewell *et al.*,[8] Ivey[9] and Nicolette *et al.*[10] using water or a glycerol–water mixture for a range of Rayleigh numbers up to $1{\cdot}49 \times 10.^9$ The results with mercury showed that the temperature oscillates at a low frequency with a small amplitude. The amplitude of the oscillation is location-dependent. Both the frequency and amplitude increase with increasing temperature difference. Oscillations were not observed for $Gr \leq 1 \times 10^6$ in a cavity with an aspect ratio of one.[7,11] Inconsistent results were obtained with water and with a gylcerol–water mixture. Experiments by Yewell *et al.*[8] did not reveal any oscillations in the flow regardless of the high Rayleigh number ($1{\cdot}4 \times 10^9$) and the location of the probe. In contrast, Ivey[9] observed oscillations in temperature at $Ra = 3{\cdot}9 \times 10.^8$ This oscillatory

0271–2091/91/110061–21$10.50

Received April 1989
Revised July 1990

flow approached the final steady state conditions for certain flow regimes. No correlation was found between two temperature records at locations very near to each other. The author argued that this oscillation is due to the inertia of the flow entering the interior of the cavity from the side wall boundary layer, which leads to a hydraulic jump.

For direct numerical simulation of transient thermal convection in low-Pr fluids, we refer to a number of pioneering papers[12-17] using a variety of methods. For example, oscillatory convection was predicted for a liquid metal ($Pr=0{\cdot}005$) confined to a square cavity ($A=1$) at a Grashof number of 1×10^7, but a critical Grashof number for oscillatory convection was not determined.[14] Weak secondary flows were predicted in the corners of the cavity.[13,14] Examination of the available results for low-Pr fluids reveals that the determination of the threshold of oscillatory convection with direct simulation is difficult because it is strongly mesh-dependent.

Numerical predictions of steady state thermal convection in low-Prandtl-number fluids have been made by different authors for steady state conditions. A unicellular motion was predicted[7,11] to exist in the cavity for $Gr<1\times10^6$. One interesting observation from the results of Stewart and Weinberg[18] is that the streamlines are almost square for high-Prandtl-number ($Pr=10$) fluids, while they are almost circular for low-Prandtl-number ($Pr=0{\cdot}013$) flows. There may exist small secondary circulations in the corners of the cavity, which are not predicted because of the coarse mesh (21×21) used in the analysis.

The problem of predicting the flow field in low-Prandtl-number fluids due to thermal buoyancy force is not well understood. The flow is highly non-linear, because the inertial force dominates the flow, and the viscous effects are mainly confined to the very thin boundary layers. Experimental diagnostic techniques for low-Prandtl-number fluids (i.e. liquid metals) may introduce significant errors due to non-wetting between the metal and the measuring probe. Flow visualization is not possible owing to the opaqueness of the metal, and the use of radioactive tracers is possible but difficult. On the other hand, numerical simulations may produce an erroneous flow field if the algorithm is not adequate. There is a lack of experimental and theoretical results for the thermally driven flow of low-Prandtl-number fluids, under transient conditions.

This paper deals with a two-dimensional numerical simulation of transient natural convection in a differentially heated square cavity. The numerical study has been undertaken as a first step, because the flow of liquid metals and semiconductors cannot be visualized and velocity measurements in buoyancy-driven liquid metal flows at low velocities are exceedingly difficult. This work is motivated by the need to gain a fundamental understanding of the physics and the onset of instability in a differentially heated square cavity filled with a low-Prandtl-number fluid. The work is relevant to solidification of ingots and castings, crystal growth from melts, materials processing, nuclear reactor safety and other applications. The effects of the Prandtl number on the flow structure and heat transfer are studied.

ANALYSIS

Physical and mathematical model

We study the behaviour of homogeneous low-Prandtl-number fluids subjected to a buoyancy force inside the two-dimensional rectangular cavity of height H and length L ($A=L/H$ is the aspect ratio) shown in Figure 1. The isothermal vertical walls are kept at constant but different temperatures, while the upper and lower connecting walls are adiabatic. Initially the fluid is at the cold wall temperature, then suddenly at times $t=0$ the temperature of one of the vetical walls is increased to a constant value $T_h>T_c$. The convective flow is generated by the buoyancy force as soon as $T_c\neq T_h$. The intensity of the convective flow depends on the magnitude of the temperature

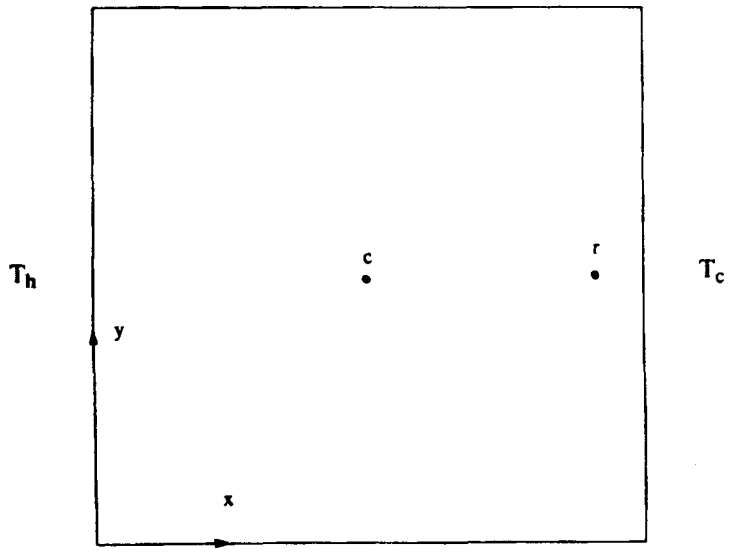

Figure 1. Schematic diagram and co-ordinate system of the cavity

difference $\Delta T = T_h - T_c > 0$. The fluid within the cavity is assumed to have constant properties, except where buoyancy is concerned, i.e. the Boussinesq approximation is assumed to be valid. Scales of ΔT, H, H^2/α and α/H are used for temperature, length, time and velocity respectively.

The governing conservation equations can be written as

$$\nabla \cdot \bar{\mathbf{V}} = 0, \tag{1}$$

$$Pr^{-1}\left(\frac{\partial \bar{\mathbf{V}}}{\partial \tau} + \bar{\mathbf{V}} \cdot \nabla \bar{\mathbf{V}}\right) = -Pr^{-1}\nabla P + \nabla^2 \bar{\mathbf{V}} - Ra\theta \mathbf{j}, \tag{2}$$

$$\frac{\partial \theta}{\partial \tau} + \nabla \cdot (\bar{\mathbf{V}}\theta) = \nabla^2 \theta, \tag{3}$$

where ∇ and ∇^2 are the gradient and Laplacian operators respectively. In equations (1)–(3), $\bar{\mathbf{V}} = (\mathbf{i}U + \mathbf{j}V)$ is the dimensionless velocity vector, P is pressure, θ is temperature, τ is dimensionless time and $Pr\,(=\nu/\alpha)$ and $Ra = GrPr = (g\beta\Delta T H^3/\nu\alpha)$ are the Prandtl and Rayleigh numbers respectively. The dimensionless co-ordinates ξ and η are defined as x/L and y/H respectively (see Figure 1).

The boundary conditions are taken as

$$\theta = 1 \quad \text{at } \xi = 0, \tag{4}$$

$$\theta = 0 \quad \text{at } \xi = 1, \tag{5}$$

$$\frac{\partial \theta}{\partial \eta} = 0 \quad \text{at } \eta = 0, 1, \tag{6}$$

$$\bar{\mathbf{V}} = 0 \quad \text{at all the boundaries.} \tag{7}$$

Method of solution

Various methods have been used to solve the above transport equations. Finite difference,[18,19] finite element,[14,15] finite analytic[20] and spectral[21] methods have been employed using either streamfunction–vorticity or primitive variables approaches. In this paper a primitive variables approach is used to solve the finite difference form of equations (1)–(7). The domain of interest is divided into non-uniform control volumes. The mesh is staggered in such a way that the velocities calculated at the points lie on the faces of the control volumes, while the temperature is calculated at the midpoint of the control volumes.[22] The difference equations are obtained by integrating the equations over each control volume. Non-linear algebraic equations resulting from discretization are solved iteratively using a tridiagonal matrix algorithm. A backward-Euler (implicit) time-differencing scheme is used to march the solution foward in time. Each time step advances the solution after a convergence is achieved. Two criteria were checked to insure the convergence of the solution. They included the ficticious mass source in the continuity equation[22] convergence to zero, $O(1\times10^{-6})$, and convergence of certain selected arbitrary velocities and temperatures to constant values.

Central difference discretization of the diffusive–advective flux is used for spatial derivatives, with a truncation error $O(\Delta\tau,\Delta x^2)$. The results are based on the central difference discretization, which is second-order-accurate, and are compared with the results based on the power-law scheme, which is an approximation for the one-dimensional exact solution. The power-law scheme showed more dumping on the amplitude of the oscillation than the central difference owing to false diffusion. This is consistent with results of Bottaro and Zebib.[23] Also, Patel and Markatos[24] concluded that the power-law scheme can be inaccurate for course grids. Hence the central difference scheme is used.

Non-uniform grids are generated by applying a sine function property, which produces fine meshes near the walls that gradually increase in size up to the centre of the cavity. The location of the mesh points is calculated from

$$x_{i+1}=x_i+C\sin\left[\frac{\pi(i-1)}{L_N-1}\right], \tag{8}$$

where the constant C can be found by integration:

$$x_L=\int_0^{L_N} C\sin\left[\frac{\pi(i-1)}{L_N-1}\right]\mathrm{d}i \tag{9}$$

or

$$C=\frac{x_L\pi}{2(L_N-1)}. \tag{10}$$

In this equation x_L is the x-axis length and L_N is the number of nodes in the x-direction. A similar procedure is used to locate the meshes along the y-axis. Figure 2 shows the 61×61 mesh generated using the above equations. Non-uniform meshes of 21×21, 31×31, 41×41, 51×51, 61×61 and 81×81 are considered in order to establish grid independence of the results.

The results of three non-uniform meshes of 41×41, 61×61 and 81×81 for $Gr=1\times10^7$ and $Pr=0{\cdot}005$ were compared and revealed insignificant difference in the streamlines and isotherms (Figure 3) for 61×61 and 81×81. The time series of velocity fields and Nusselt numbers showed little difference, except that there is a small shift in the average value of the U-velocity at the centre of the cavity and in the average Nusselt number at the vertical walls of the cavity (Figure 4). The

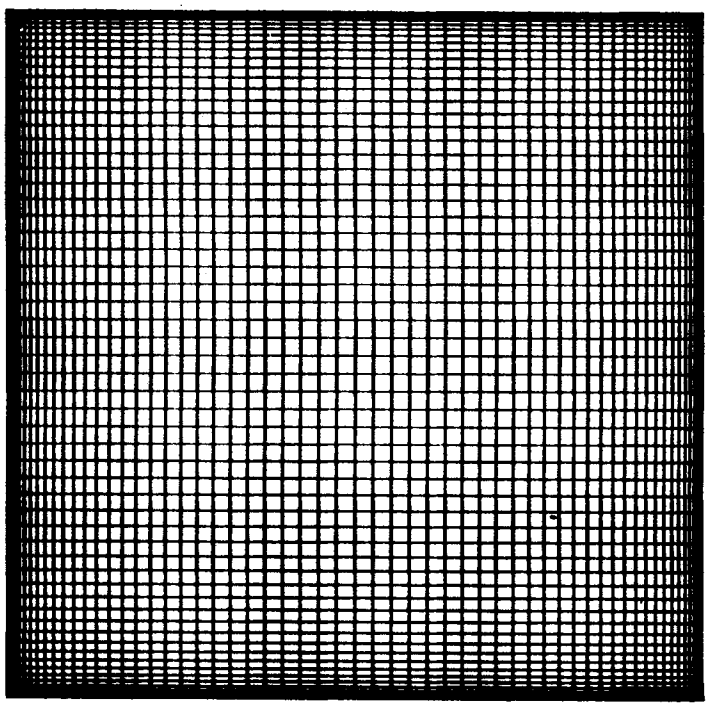

Figure 2. A 61 × 61 non-uniform mesh distribution

average Nusselt number at the vertical walls is calculated as

$$Nu = -\int_0^1 \left.\frac{\partial\theta}{\partial\xi}\right|_{\xi=0,1} \mathrm{d}\eta. \tag{11}$$

The effect of the spatial resolution on the average Nusselt number at the vertical walls of the cavity, after steady state oscillation has been established, is shown in Figure 4. The trend of the time series for the Nusselt number is the same for meshes 41 × 41, 61 × 61 and 81 × 81, except that the values for mesh 41 × 41 underpredict the Nusselt number. Note the very fine ordinate scale on the enlarged plot (Figure 4). The difference between the average Nusselt number predicted by the 61 × 61 and 81 × 81 meshes is 0·48% and between the 41 × 41 and 81 × 81 meshes it is 1·69%. The difference in frequency of the oscillation is less than 1% for the 61 × 61 and 81 × 81 meshes. Therefore it is assumed that the 61 × 61 non-uniform mesh is sufficiently fine. In fact, for $Gr = 1 \times 10^7$ and $Pr = 0{\cdot}005$ the frequency is above the threshold of oscillation. Hence all the calculations were carried with 61 × 61 non-uniform meshes until the lower bound was reached; then the number of grids was increased to 81 × 81 and the time step was reduced to one-half of that used for the 61 × 61 mesh to insure grid-independent results.

Time steps of 0·001, 0·002 and 0·004 were tested for the 61 × 61 mesh and the predictions were found to be consistent. Hence most calculations were carried out using a time step of 0·002. This insures that there are more than 30 time steps for the resolution of one cycle of oscillation (i.e. no aliasing effect). For $Pr = 0{\cdot}01$ the time step was reduced to 0·0005, because at the same Grashof number the oscillation frequency was higher than that for $Pr = 0{\cdot}005$. However, for $Pr = 0{\cdot}001$ the oscillation frequency was low, and the tests showed that even using a time step of 0·01 yields

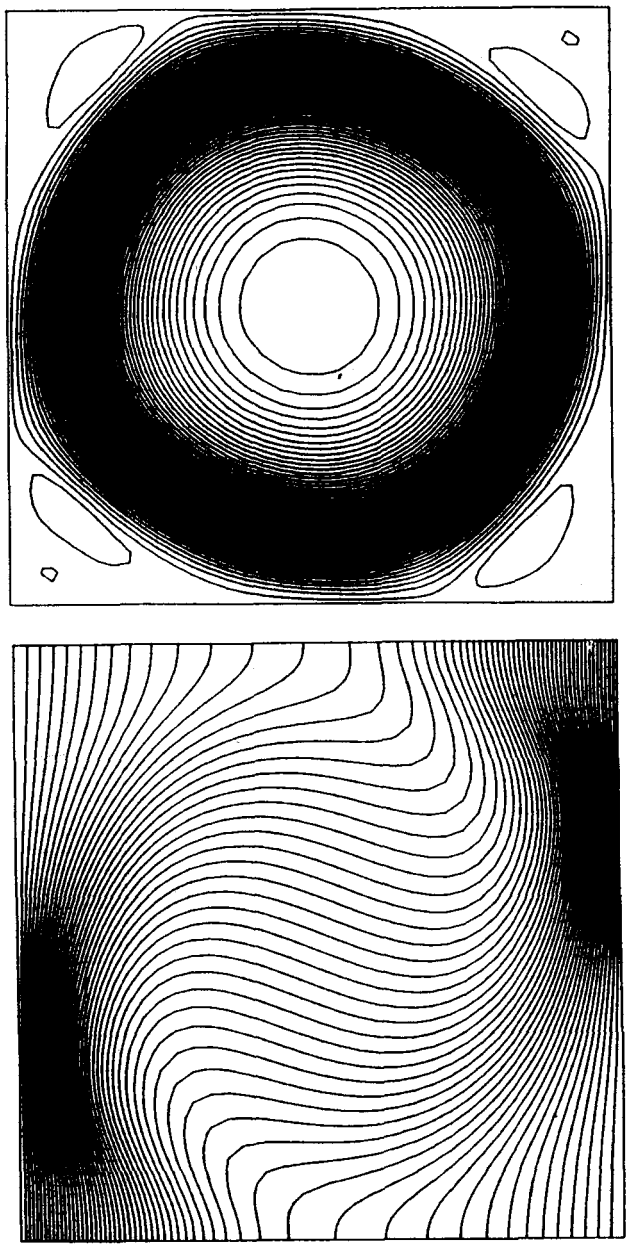

Figure 3. Streamlines and isotherms for $Pr = 0{\cdot}005, Gr = 1 \times 10^7$ at $\tau = 6$; $\psi_{min} = -6{\cdot}6029$, $\psi_{max} = 0{\cdot}2109$

insignificant differences compared with time steps of 0·002 and 0·001. Therefore the time step used in most of the calculations was 0·002 or 0·001 to insure that more than 30 time increments were used to resolve the fine time scale of oscillation for one period. All the calculations were carried on a Gould mini-super computer. The CPU time for each time step per node was 0·03 s when using an implicit double-precision method to reduce the round-off error.

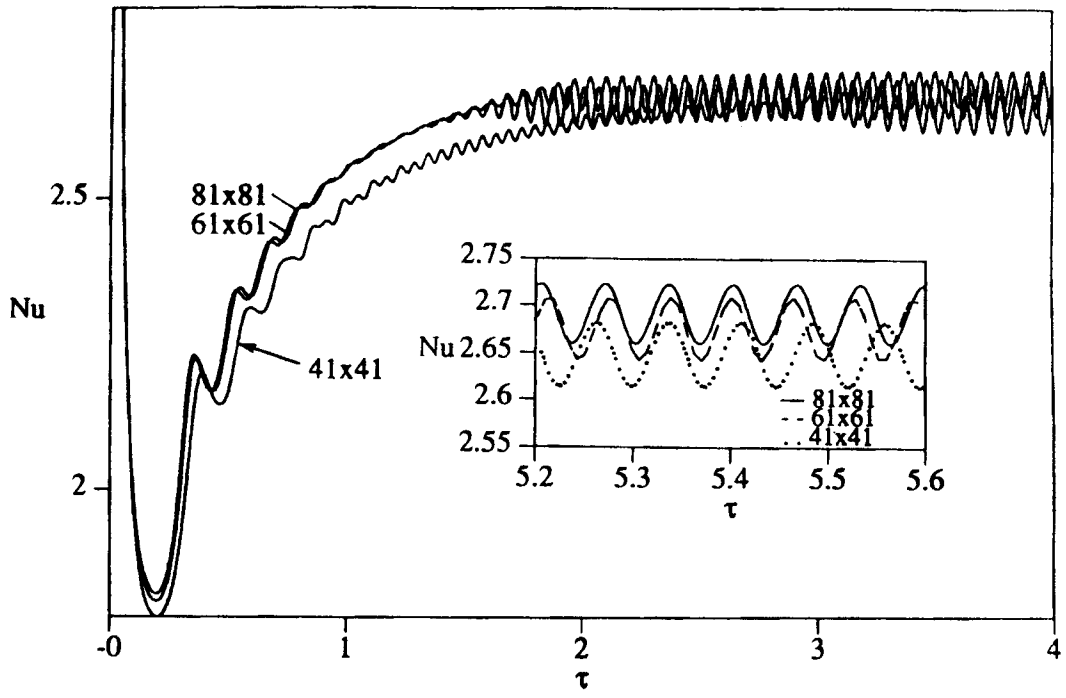

Figure 4. Comparison of the average Nusselt number at the vertical walls of the cavity for meshes of 41×41, 61×61 and 81×81 with $Pr = 0{\cdot}005$ and $Gr = 1 \times 10^7$

RESULTS AND DISCUSSION

All the calculations began with a stagnant fluid, and the temperature of the left vertical wall was suddenly increased to a constant value for $\tau \geq 0$. Fifty-five streamlines are used to plot the flow field. Such a high resolution is intended to identify small-scale structures in the flow. This is important to understand the physics of the flow. Also, the minimum and maximum values of the streamlines are given in the figure captions at the specified time for the purpose of comparison with other schemes. If the steady state solution was achieved, the Nusselt numbers are given on the figure, truncated to the number of significant figures that converged.

Results for $Pr = 0{\cdot}001$

For $Pr = 0{\cdot}001$ and $Gr = 1 \times 10^6$ no oscillation was predicted. The basic flow is a one-cell circulation limited by the lateral confinement. The flow and temperature fields gradually approached steady state. An increase of the Grashof number to 2×10^6 yielded oscillatory flows with a very low frequency. A very long time simulation was required to predict whether the oscillation decays or amplifies (which took several days of computer time in time-sharing systems). Figure 5 shows the variation of the U-velocity at the centre of the cavity with time. It should be noted that using a mesh of 81×81 yields no difference in total and global variables compared with the results obtained when a mesh of 61×61 was employed for $Gr = 2 \times 10^6$. The Nusselt number did not yield a converged value but increased very slowly (within the fourth decimal digit) with time at both vertical walls of the cavity (Figure 6). For $Gr = 3 \times 10^6$ the oscillatory transient period was followed by an oscillating flow (Figure (7a)). This is displayed for the U-velocity at the centre

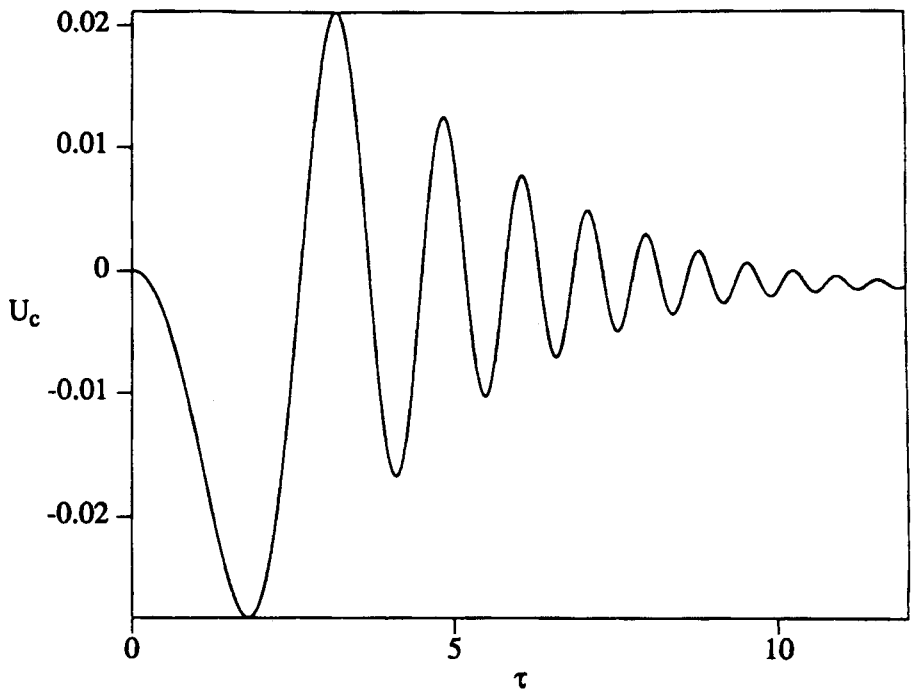

Figure 5. Time series of U-velocity at the centre of the cavity for $Pr=0{\cdot}001$ and $Gr=2\times10^6$

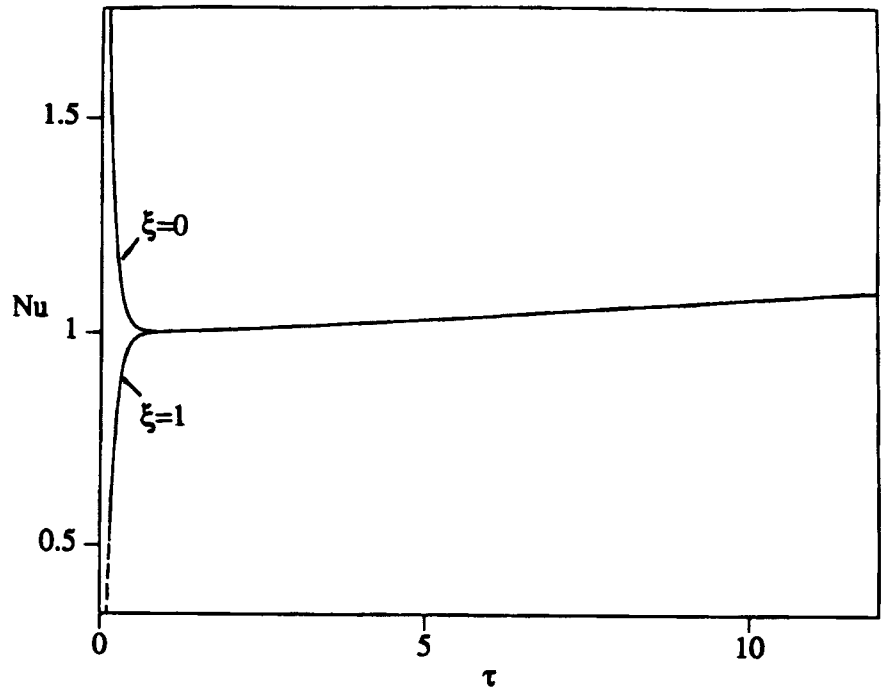

Figure 6. Time series of the average Nusselt number at both vertical walls of the cavity for $Pr=0{\cdot}001$ and $Gr=2\times10^6$

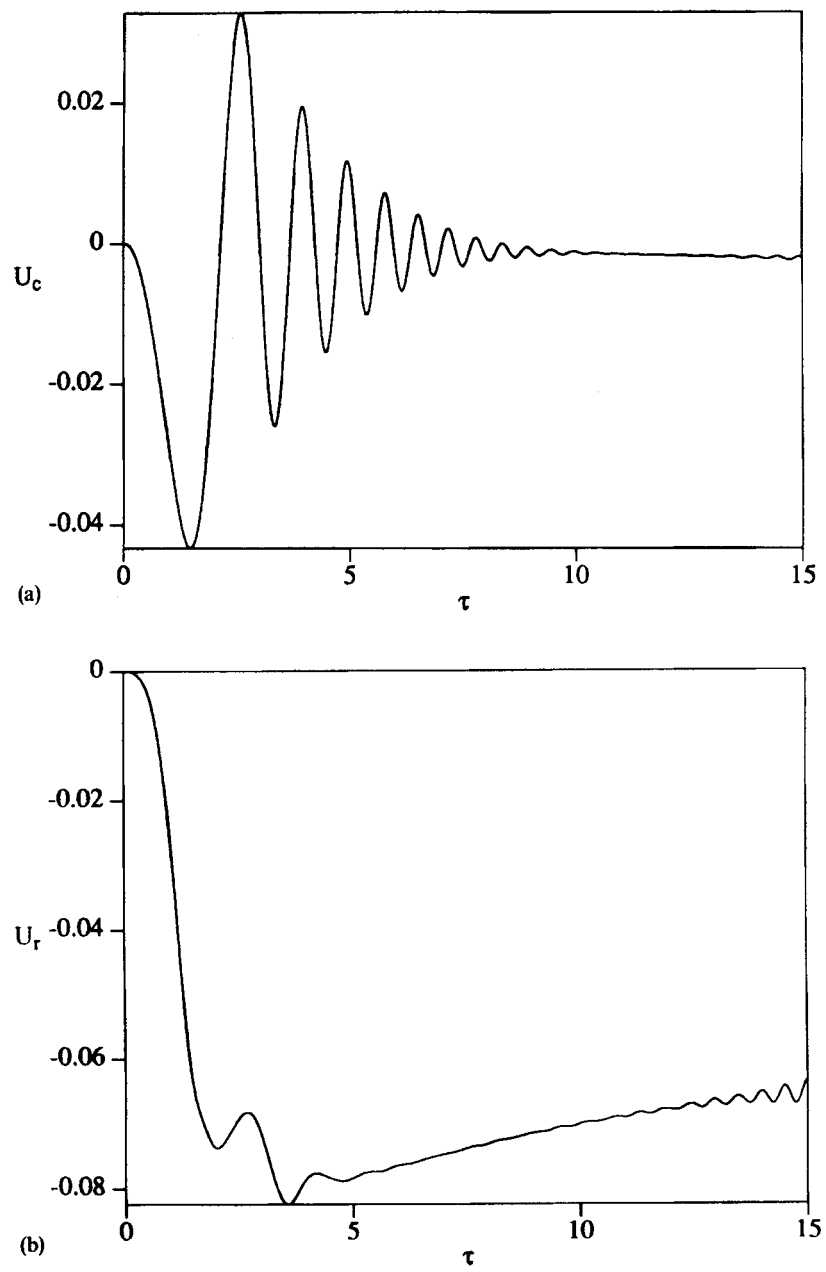

Figure 7. Transient U-velocities for $Pr=0{\cdot}001$ and $Gr=3\times10^6$: (a) at the centre of the cavity; (b) at the mid right-hand corner of the cavity

of the cavity. It should be mentioned that all the locations in the cavity revealed similar trends and differed only in amplitude. For example, Figure 7(b) shows the U-velocity time series at the mid-cavity near the right boundary (see Figure 1 for location) and reveals that the onset of oscillation is the same as in Figure 7(a). Similar findings were obtained for other Grashof and Prandtl numbers

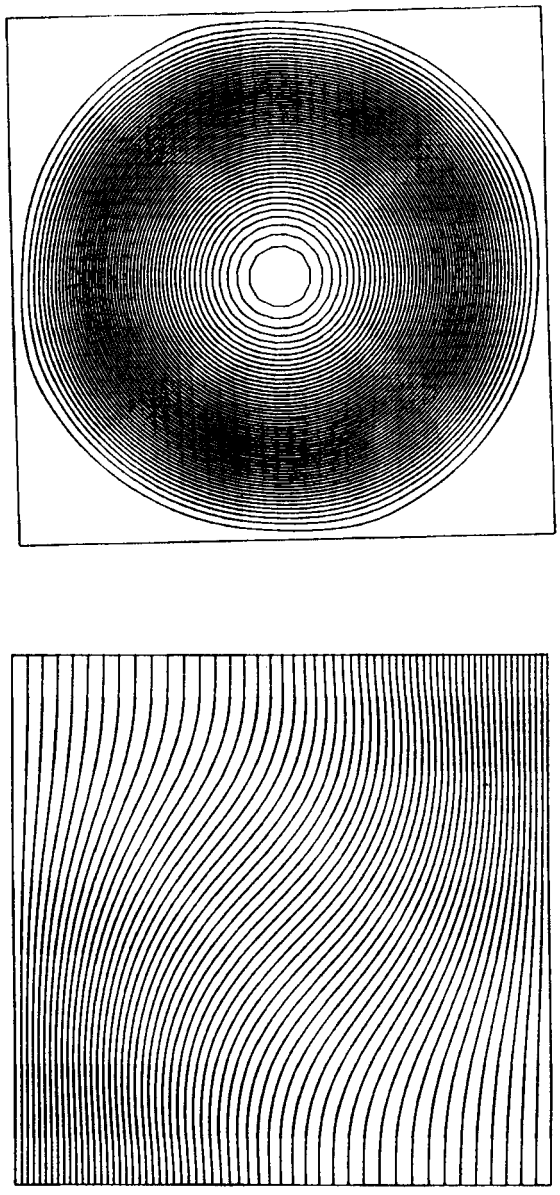

Figure 8. Streamlines and isotherms for $Pr=0{\cdot}001$, $Gr=3\times10^6$ at $\tau=15$; $\psi_{min}=-1{\cdot}6399$, $\psi_{max}=0{\cdot}0101$

when the flow field oscillates at the same frequency and only the amplitude is location-dependent. The Nusselt number did not show convergence (with variation in the fourth decimal point) but varied slowly even when the calculations were carried to $\tau=15$. Streamlines revealed one main circulation (Figure 8), and probably very weak circulations in the corners were present but cannot be resolved with 55 streamlines; however, the minimum and maximum values of the streamlines indicate very weak circulations.

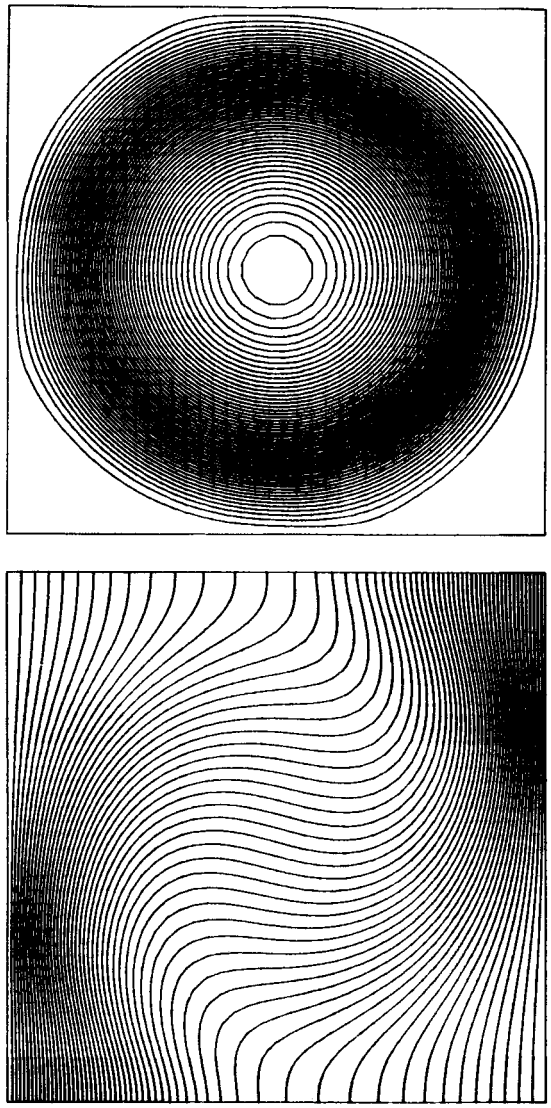

Figure 9. Streamlines and isotherms for $Pr=0{\cdot}005$, $Gr=3\times10^6$ at $\tau=8$; $\psi_{min}=-5{\cdot}2402$, $\psi_{max}=0{\cdot}0361$

Results for $Pr=0{\cdot}005$

For $Pr=0{\cdot}005$ and $Gr=1\times10^6$ the time series for velocity and temperature showed a gradual approach to a steady state solution without any oscillation. The results for $Gr=3\times10^6$ (shown in Figure 9) reveal that the streamlines are almost circular in shape, with one main circulation. Very weak circulations are probably present at the corners, as revealed by the maximum and minimum values of the streamlines. Because the negative values of the streamline indicate clockwise circulation and positive values indicate counterclockwise circulation, a comparison of Figures 8 and 9 reveals very clearly the effect of the Prandtl number on the isotherms. The time history of the flow field is shown in Figure 10. The duration of the transient stage needed to reach steady state is

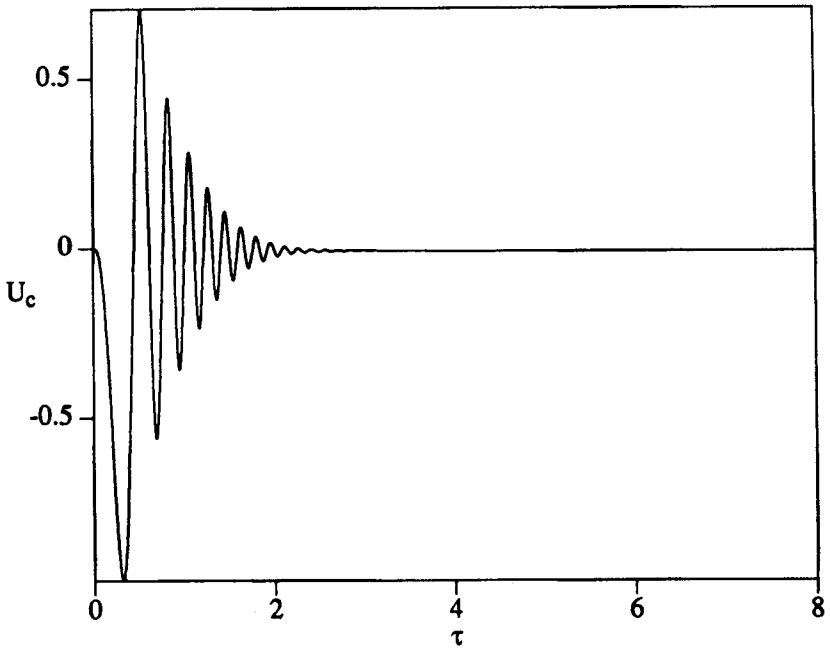

Figure 10. Time series of U-velocity at the centre of the cavity for $Pr = 0{\cdot}005$ and $Gr = 3 \times 10^6$

$\tau \approx 3$. The average Nusselt numbers at both vertical walls of the cavity converge to 2·1013 (Figure 11). The same results were obtained with an 81×81 mesh.

For $Gr = 5 \times 10^6$ the flow field at all locations oscillates with a dimensionless frequency $(1/\tau)$ of 12·2 (Figure 12), and so does the average Nusselt number (Figure 13). The corner circulations are evident in Figure 14. A comparison of the streamlines depicted in Figures 3 and 14 clearly shows that the streangth of these oscillations increases with the Grashof number. We should emphasize that we performed the computations for long periods of time during which the solution behaviour remained unchanged. However, we do not claim that the solution will exhibit the same behaviour if the computation is extended.

It should be mentioned that Benocci[13] predicted oscillatory flow for $Pr = 0{\cdot}005$ at $Gr = 1 \times 10^7$, whereas our results reveal oscillating flow for $Gr > 3 \times 10^6$. Also, Benocci's results do not show skew symmetry in the streamlines. This discrepancy may be explained by the fact that Benocci[13] used a coarser mesh (31×31), resulting in an overestimation of the threshold value. However, it is difficult to compare our results with those of Benocci, because he did not indicate explicity that $Gr = 1 \times 10^7$ is the critical value, and the frequency of the oscillation was not given.

Results for $Pr = 0{\cdot}01$

Using 81×81 meshes for $Pr = 0{\cdot}01$ and $Gr = 1 \times 10^7$ with a time step of 0·0005, the streamlines reveal one main circulation with two rotating cells inside the main circulation, in addition to the corners cells (Figure 15). Spectral analysis showed two frequencies with their interaction after eliminating the transient period. The power content of the frequencies is location-dependent as seen in Figures 16(a) and 16(b), which show the time series with power spectra of the U-velocity at the centre and mid-right of the cavity respectively. The fundamental frequency is 21·5 and the

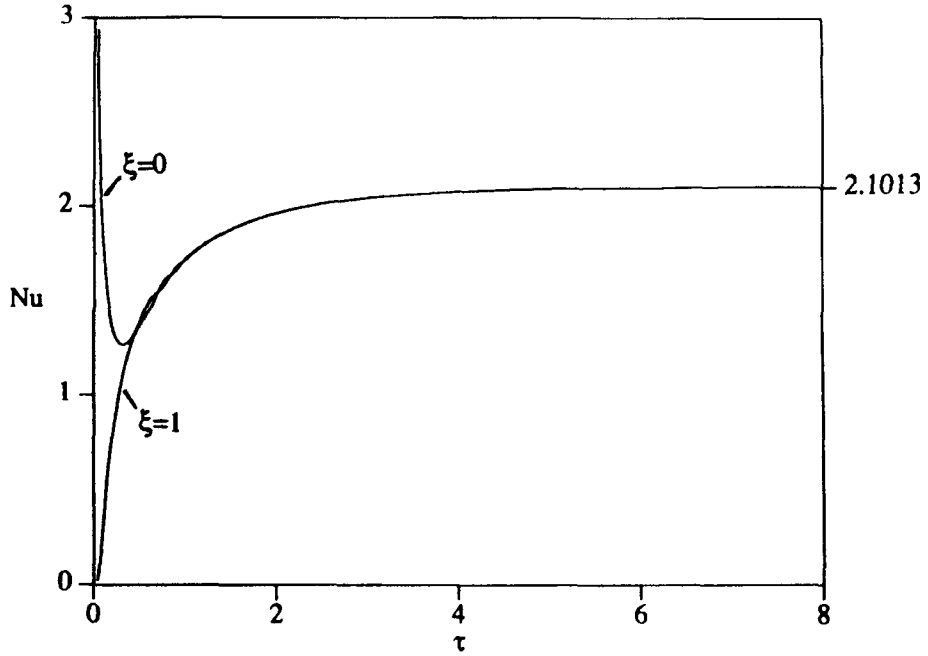

Figure 11. Time series of the average Nusselt number at both vertical walls of the cavity for $Pr=0{\cdot}005$ and $Gr=3\times10^6$

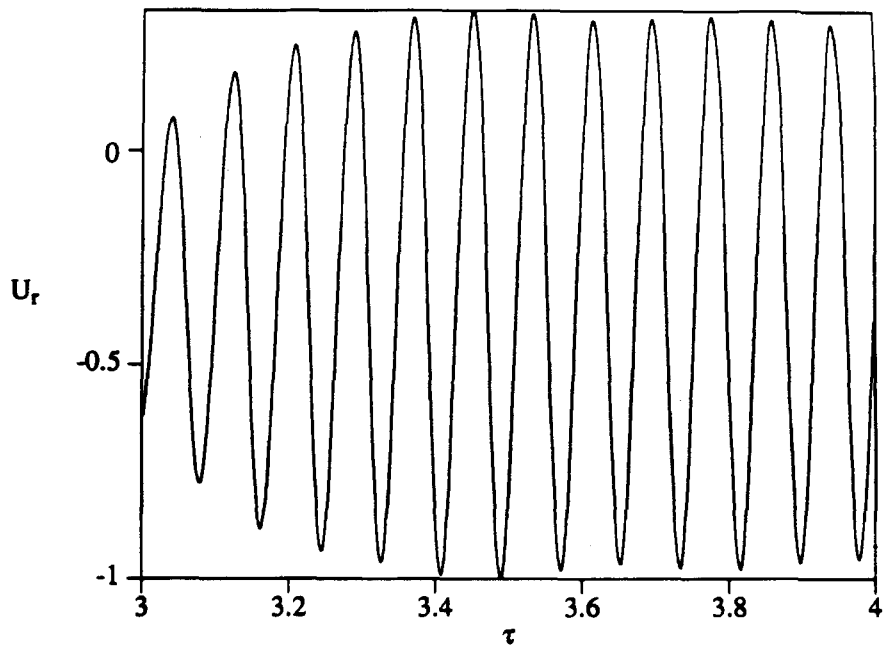

Figure 12. Time series of U-velocity at mid right-hand corner of the cavity for $Pr=0{\cdot}005$ and $Gr=5\times10^6$

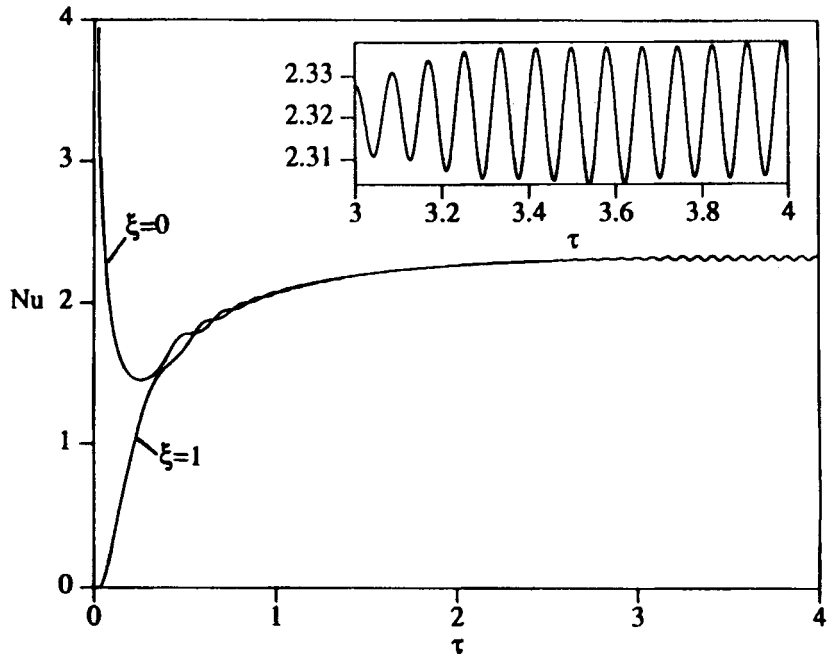

Figure 13. Time series of the average Nusselt number at both vertical walls of the cavity for $Pr = 0{\cdot}005$ and $Gr = 5 \times 10^6$

Table I. Summary of the numerical results

Pr	Gr	τ	ψ_{min}	ψ_{max}	Nu†	Dimensionless frequency
0·001	2×10^6*	12	−1·0096	0·0065	1·2142	
	3×10^6	15	−1·6399	0·0101	1·2178	
0·005	3×10^6*	8	−5·2402	0·0361	2·1013	
	5×10^6	4	−5·8162	0·1647	2·3210	12·2
	1×10^7	6	−6·6029	0·2109	2·6863	15·9
0·01	5×10^6*	3	−6·9119	0·0596	2·8143	
	1×10^7	2	−7·8938	0·0970	3·2344	21·5

* Oscillation was predicted for Gr greater than the indicated value.
† Nusselt number averaged over time for oscillatory flow.

secondary frequency is 13·8. In a numerical simulation, Gresho and Upson,[14] using 70×70 uniform element meshes, predicted similar phenomena. Decreasing the Grashof number to 8×10^6 also revealed oscillation as seen in Figure 17, which is a time series of the centre U-velocity. However, at $Gr = 5 \times 10^6$ a decaying oscillatory transient was predicted and the flow approached steady state. Figure 18 displays the time series of the U-velocity at the centre of the cavity. All locations inspected and the Nusselt number showed a similar trend. Streamline plots reveal a cell at the upper right-hand corner and by skew symmetry at the lower left-hand corner cavity, in

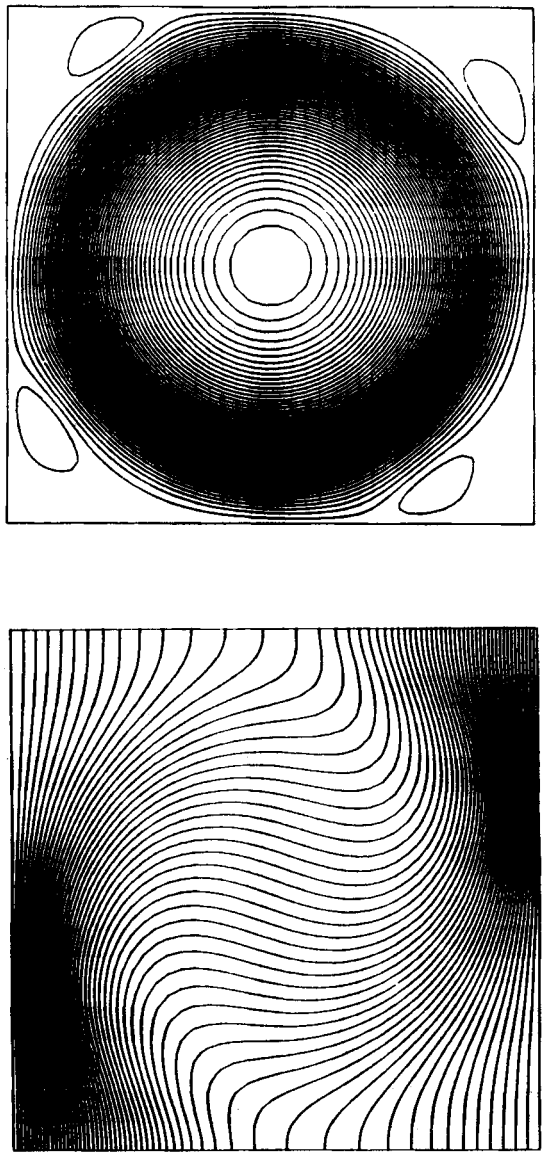

Figure 14. Streamlines and isotherms for $Pr=0{\cdot}005$ and $Gr=5\times10^6$ at $\tau=4$; $\psi_{min}=-5{\cdot}0162$, $\psi_{max}=0{\cdot}1647$

addition to the main circulation (Figure 19). Hence it is considered that $Gr=5\times10^6$ is the threshold value. It should be mentioned that all the calculations for $Pr=0{\cdot}01$ were carried out with an 81×81 mesh and a time step of 0·0005. The value of $Gr=5\times10^6$ is much larger than the value of $5{\cdot}91\times10^4$ for $A=4$ and $Pr=0{\cdot}015$ which is reported by Winters.[15] However, as indicated by Winters, the critical value increases to $3{\cdot}10\times10^5$ if the aspect ratio is decreased to 2·4. Hence a decrease in the aspect ratio is expected to increase the critical Grashof number for the onset of oscillation and may change the mode of instability.

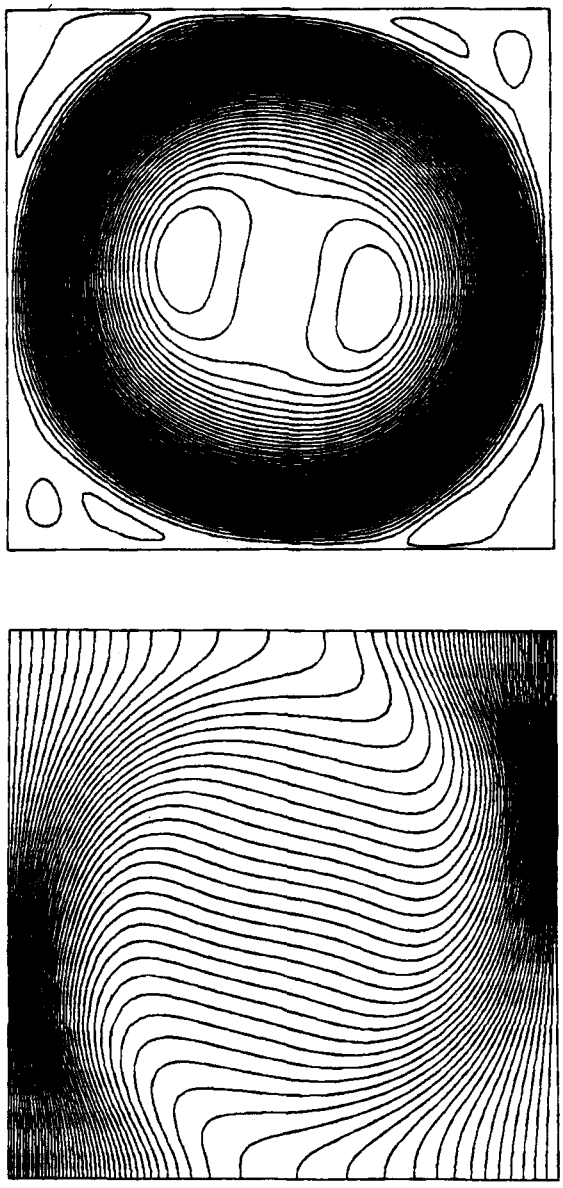

Figure 15. Streamlines and isotherms for $Pr=0{\cdot}01$ and $Gr=1\times10^7$ at $\tau=2$; $\psi_{min}=-7{\cdot}8938$, $\psi_{max}=0{\cdot}0970$

Comparison of results for different Prandtl numbers

Table I summerizes the results of the predictions. A comparison of the results for $Pr=0{\cdot}01$, 0·005 and 0·001 shows that as the Prandtl number decreases, the period of oscillatory transient regime increases dramatically (compare Figures 5, 10 and 16). The frequency of oscillation and the critical Grashof numbers decrease as the Prandtl number decreases. The critical values of Grashof number given in this paper may serve as a starting point to obtain more precise results. One may also use the continuation method described by Winters.[15]

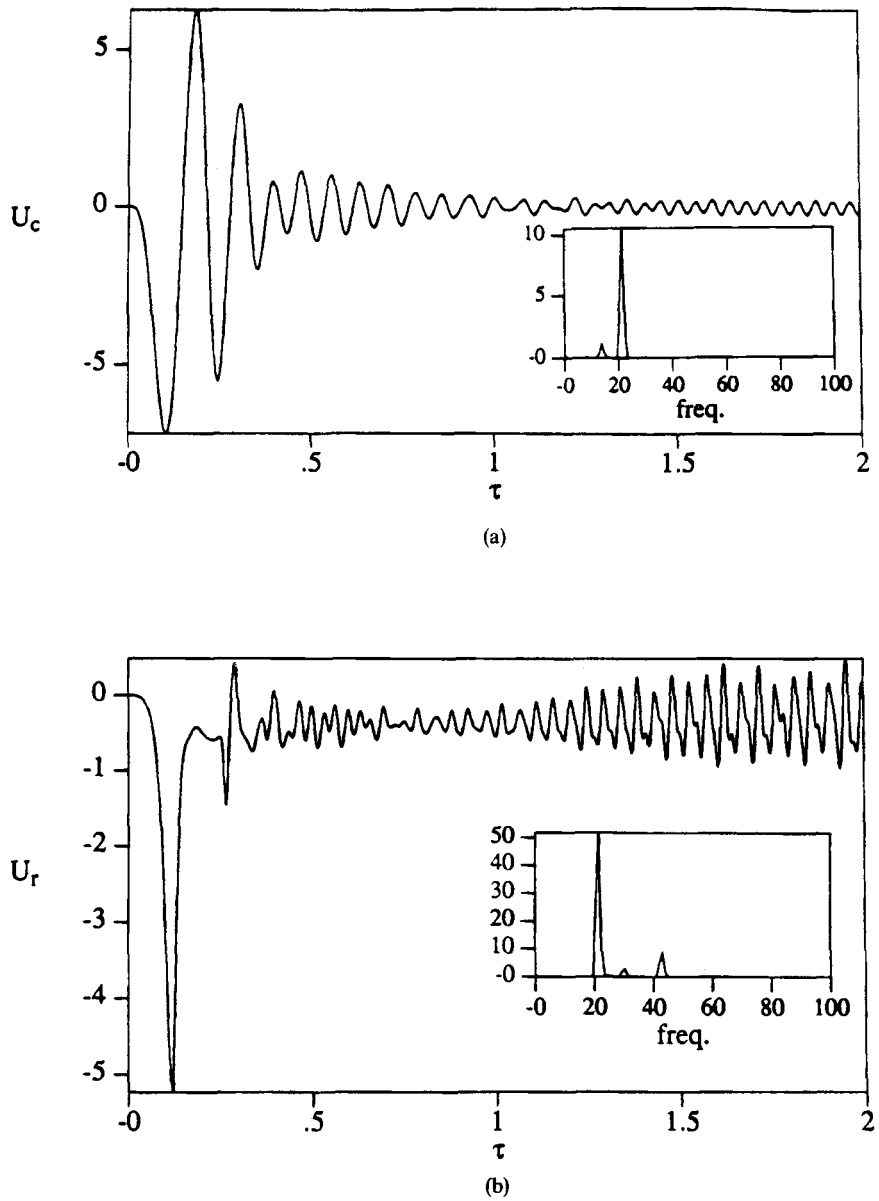

Figure 16. Time series and power spectra of U-velocity (a) at the centre of the cavity and (b) at mid-right of the cavity for $Pr = 0{\cdot}01$ and $Gr = 1 \times 10^7$

For $A = 4$ and $Pr = 0{\cdot}015$, Winters,[15] using a technique which locates Hopf bifurcation conditions from a finite element solution of the extended system of equations, predicted a threshold value $Gr = 5{\cdot}91 \times 10^4$ for oscillatory convection, whereas Crochet *et al.*,[16] using direct numerical simulation, predicted a value $Gr = 3{\cdot}2 \times 10.^5$ However, it is not known if the Grashof number of $3{\cdot}2 \times 10^5$ in the work of Crochet *et al.* is the ciritical value, because they have not performed the computations for many values of Gr. There is a similar discrepancy between the

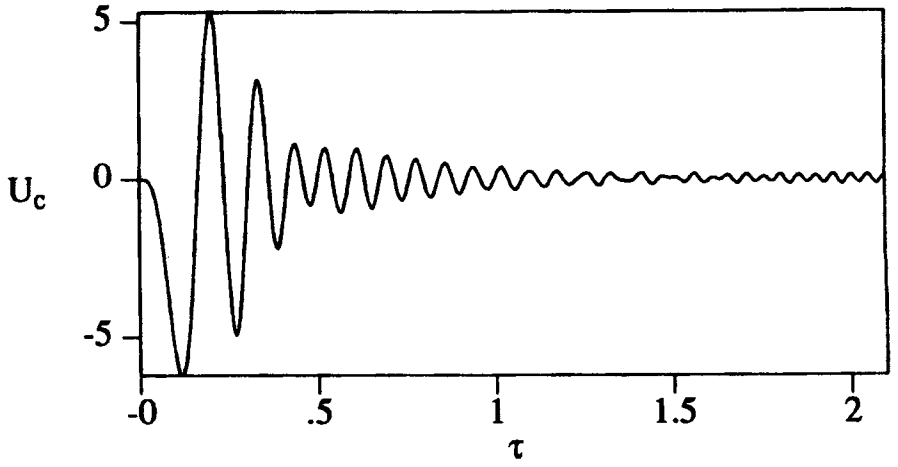

Figure 17. Time series of U-velocity at the centre of the cavity for $Pr=0{\cdot}01$ and $Gr=8\times10^6$

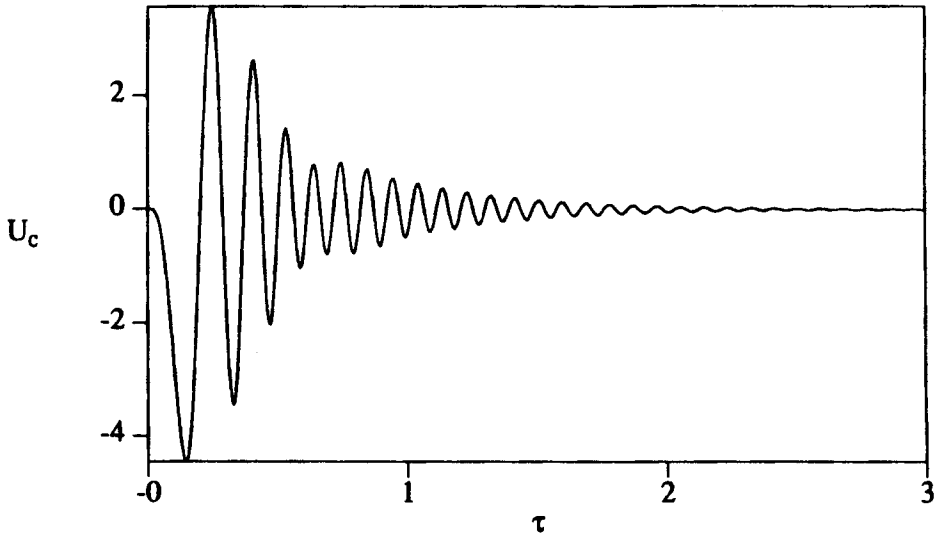

Figure 18. Time series of U-velocity at the centre of the cavity for $Pr=0{\cdot}01$ and $Gr=5\times10^6$

results of Bottaro and Zebib[23] and Crochet *et al.*[25] It is clear from the results reported that accurate determination of the threshold of oscillatory convection by direct simulation is very delicate, because it is very strongly mesh-dependent. Coarse meshes may result in the stabilization of the solution and in the delay of the onset of oscillatory convection at a higher value of Grashof number and with a damped amplitude of oscillation. Hence a wide spread is found among the critical Grashof numbers determined from direct numerical simulations and disagreement with the results based on stability analysis.

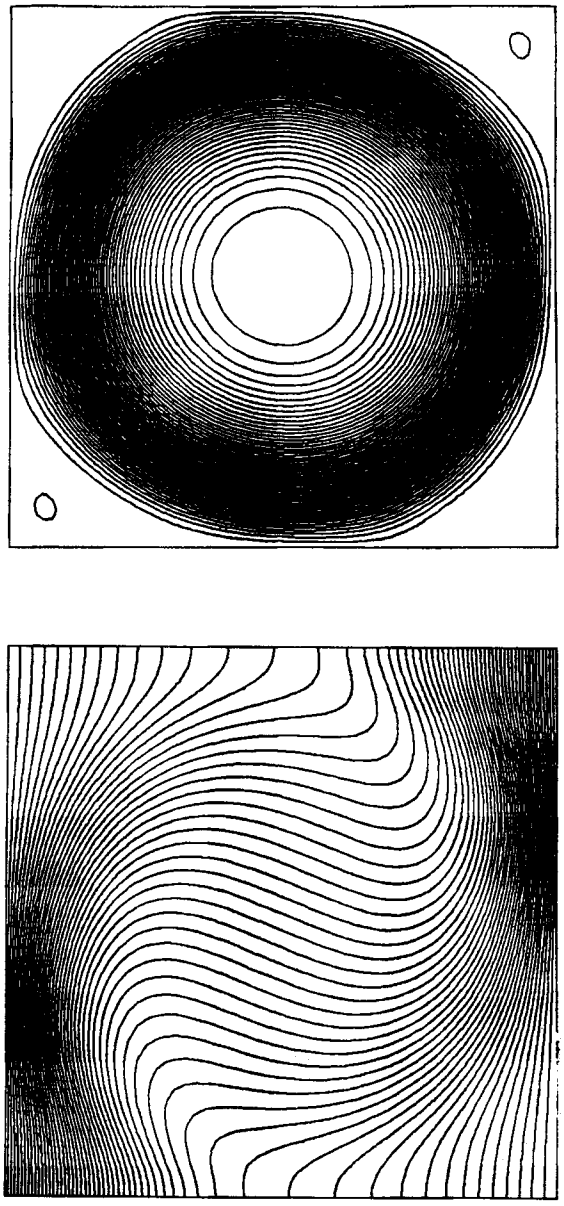

Figure 19. Streamlines and isotherms for $Pr = 0{\cdot}01$ and $Gr = 5 \times 10^6$

CONCLUSIONS

This paper has reported numerical results for transient natural convection in a differentially heated square cavity for $Pr = 0{\cdot}001$, $0{\cdot}005$ and $0{\cdot}01$. The control volume approach was used to formulate the finite difference form of the conservation equations, with a truncation error $O(\Delta\tau, \Delta x^2)$. The calculations were carried out in double precision. For a square cavity ($A = 1$) a finite set of Grashof numbers has been investigated. A finite time of integration has been

considered for unsteady calculations. These facts must be kept in mind when the following conclusions are drawn.

1. For $Gr = 1 \times 10^6$ with $Pr = 0{\cdot}001$ and $0{\cdot}005$ the results showed that the flow field asymptotically approaches steady state.
2. Damped oscillatory transient periods were predicted for $Pr = 0{\cdot}001$, $0{\cdot}005$ and $0{\cdot}01$ at Grashof numbers of 2×10^6, 3×10^6 and 5×10^6 respectively.
3. Periodic flow was predicted for $Pr = 0{\cdot}001$, $0{\cdot}005$ and $0{\cdot}01$ at Grashof numbers of 3×10^6, 5×10^6 and 8×10^6 respectively.
4. The frequency of oscillations and the ciritical Grashof number decrease as the Prandtl number decreases.
5. Four weak circulation cells were predicted at the corners of the cavity. The strength of the cells in the upper right-hand and lower left-hand corners is greater than the strength of the upper left-hand and lower right-hand circulations. The results showed that the upper right-hand and lower left-hand corner vortices evolved first, followed by the vortices in the other two corners. This finding is consistent with the results of Gresho and Upson.[14] This may suggest that the origin of the stability first appears at the upper right-hand corner and is due to the skew symmetry at the lower left-hand corner.

REFERENCES

1. L. D. Landau and E. M. Lifschitz, *Fluid Mechanics*, Pergamon, London, 1959.
2. B. Gebhart, Y. Jaluria, R. L. Mahajan and B. Sammakia, *Buoyancy-Induced Flows and Transport*, Hemisphere, Washington, DC, 1988.
3. M. Pimputkar and S. Ostrach, 'Convective effects in crystals grown from melts,' *J. Cryst. Growth*, **55**, 614–646 (1981).
4. W. E. Langlois, 'Buoyancy-driven flows in crystal-growth melts', *Ann. Rev. Fluid Mech.*, **17**, 191–215 (1985).
5. H. Ben Hadid, B. Roux, A. Randriamampianina, E. Crespo and P. Bontoux, 'Onset of oscillatory convection in horizontal layers of low-Prandtl number melts', in M. G. Velarde (ed.), *Physicochemical Hydrodynamics, NATO–ASI Series*, Plenum, New York, 1988, pp. 997–1028.
6. B. R. Pamplin and G. H. Bolt, 'Temperature oscillation, induced in a mercury bath by horizontal heat flow', *J. Phys. D. Appl. Phys.* **9**, 145–149 (1976).
7. Y. Kamotani and T. Sahraoui, 'Oscillatory natural convection in rectangular enclosures filled with mercury', in P. J. Marchal and I. Tansawa (eds), *Proc. 1987 ASME–JSME Thermal Engineering Joint Conf. Vol. 2*, ASME/JSME, New York/Tokyo, 1987, pp. 241–245.
8. R. Yewell, D. Poulikakos and A. Bejan, 'Transient natural convection experiments in shallow enclosures', *J. Heat Transfer*, **104**, 533–538 (1982).
9. G. N. Ivey, 'Experiments on transient natural convection in a cavity', *J. Fluid Mech.*, **144**, 389–401 (1984).
10. V. F. Nicolette, K. T. Yang and J. R. Lloyd, 'Transient cooling by natural convection in a two-dimensional square enclosure', *Int. J. Heat Mass Transfer*, **28**, 1721–1732 (1985).
11. R. Viskanta, D. M. Kim and G. Gau, 'Three-dimensional natural convection heat transfer of a liquid metal in a cavity', *Int. J. Heat Mass Transfer*, **29**, 475–486 (1986).
12. I. P. Jones, 'Low Prandtl free convection in a vertical slot', *AERE Harwell Report R-10416*, 1981–1982.
13. C. Benocci, 'Thermohydraulics of liquid metals: turbulence modeling in liquid metal free convection', *von Karman Institute Lecture Series 1983–07*, 1983.
14. P. M. Gresho and C. G. Upson, 'Application of a modified finite element method to the time-dependent thermal convection of a liquid metal', in C. Taylor, C. Johnson, J. A. Smith and W. Ramsey (eds), *Proc. 3rd Int. Conf. on Numerical Methods in Laminar and Turbulent Flow*, Pineridge, Swansea, 1983, pp. 750–762.
15. K. Winters, 'Oscillatory convection in crystal melts: the horizontal Bridgman process', *Report TP-1230, Theoretical Physics Division, Harwell Laboratory*, 1987.
16. M. J. Crochet, F. T. Geyling and J. J. Van Schaftingen, 'Numerical simulation of the horizontal Bridgman growth. Part I: Two-dimensional flow', *Int. j. numer. methods fluids*, **7**, 29–48 (1987).
17. S. Dupont, J. M. Marchal, M. J. Crochet and F. T. Geyling, 'Numerical simulation of the horizontal Bridgman growth. Part II: Three-dimensional flow', *Int. j. numer. methods fluids*, **7**, 49–67 (1987).
18. M. J. Stewart and F. Weinberg, 'Fluid flow in liquid metals, I. Theoretical analysis', *J. Cryst. Growth*, **12**, 217–227 (1972).
19. S. Paolucci and D. R. Chenoweth, 'Transition to chaos in a differentially heated vertical cavity', *J. Fluid Mech.*, **201**, 379–410 (1989).

20. C. J. Chen and H.-C. Chen, 'Finite analytical numerical method for unsteady two-dimensional Navier–Stokes equations', *J. Comput. Phys.* **53**, 209–226 (1984).
21. J. M. Vanel, R. Peyret and P. Bontoux, 'A pseudo-spectral solution of vorticity–stream-function equations using the influence matrix technique', in K. W. Morton and M. J. Banes (eds), *Numerical Methods for Fluid Dynamics II*, Clarendon, Oxford, 1986, pp. 463–475.
22. S. V. Patankar, *Numerical Heat Transfer and Fluid Flow*, Hemisphere, Washington, DC, 1980.
23. A. Bottaro and A. Zebib, 'Bifurcation in axisymmetric Czochralski natural convection', in H. H. Bau, L. A. Bertram and S. A. Korpelaa (eds), *Bifurcation Phenomena in Thermal Processes and Convection*, ASME, New York, 1987, pp. 113–119.
24. M. K. Patel and N. C. Markatos, 'A evaluation of eight discretization schemes for two-dimensional convection–diffusion equations', *Int. j. numer. methods fluids*, **6**, 129–154 (1986).
25. M. J. Crochet, P. J. Wouters, F. T. Geyling and A. S. Jordan, 'Finite element simulation of Czochralski bulk flow', *J. Cryst. Growth*, **65**, 153–165 (1983).